

# Mesoscale magnetism at the grain boundaries in colossal magnetoresistive films

Yeong-Ah Soh<sup>1</sup>, G. Aeppli<sup>1</sup>, N. D. Mathur<sup>2</sup>, and M. G. Blamire<sup>2</sup>

<sup>1</sup>*NEC Research Institute, 4 Independence Way, Princeton, NJ 08540*, <sup>2</sup>*Department of Materials Science, University of Cambridge, Cambridge CB2 3QZ, UK*

(November 15, 2018)

We report the discovery of mesoscale regions with distinctive magnetic properties in epitaxial  $\text{La}_{1-x}\text{Sr}_x\text{MnO}_3$  films which exhibit tunneling-like magnetoresistance across grain boundaries. By using temperature-dependent magnetic force microscopy we observe that the mesoscale regions are formed near the grain boundaries and have a different Curie temperature (up to 20 K *higher*) than the grain interiors. Our images provide direct evidence for previous speculations that the grain boundaries in thin films are not magnetically and electronically sharp interfaces. The size of the mesoscale regions varies with temperature and nature of the underlying defect.

Since the observation of large low-field magnetoresistance in polycrystalline  $\text{La}_{1-x}\text{A}_x\text{MnO}_3$  ( $A = \text{Ba}, \text{Ca}, \text{Sr}$ ) [1–4], where the effect was attributed to domain wall scattering or spin-polarized tunneling (SPT) between grains, much attention has been drawn to the role of grain boundaries (GBs) in the magnetotransport of manganites [5–7]. To isolate the GB contribution to magnetotransport, mesoscopic devices were patterned on  $\text{La}_{1-x}\text{A}_x\text{MnO}_3$  films grown on bicrystal substrates with an artificial GB [8–10]. Despite evidence that the GBs contribute in a crucial way to the electrical properties of colossal magnetoresistance (CMR) materials [11], there is no microscopic information on the magnetic and electronic properties of the GBs themselves. Here, we provide the first such information in the form of temperature ( $T$ )-dependent images obtained by magnetic force microscopy (MFM), which has a much higher resolution (30 nm) than other magnetic microscopies used to study manganites [12–14]. The images lead to the discovery of mesoscale regions around the GBs which have magnetic, and therefore also electronic, properties different from those away from the grain GBs. Apart from yielding an essential fact about thin transition metal oxide films, which are important both scientifically and technologically (especially where microelectronic applications are concerned), our work is significant as a demonstration of the use of force microscopy for discovering a spatially inhomogeneous  $T$ -dependent magnetic phenomenon.

We prepared our samples via the same procedures used to prepare the material for the GB magnetotransport devices [8,10]. Epitaxial  $\text{La}_{1-x}\text{Sr}_x\text{MnO}_3$  films with  $x = 0.3$  and 0.23 were grown by pulsed laser deposition on bicrystal  $\text{SrTiO}_3(001)$  substrates with an artificial GB where the crystals are misaligned by  $45^\circ$ . On one side of the artificial GB the [100] crystal axis of  $\text{SrTiO}_3$  crystal is parallel to the GB, whereas on the other side, the [100] axis is rotated by  $45^\circ$  with respect to the GB. The films are 100 nm thick. Because the lattice constant of  $\text{SrTiO}_3$  is larger than that of  $\text{La}_{1-x}\text{Sr}_x\text{MnO}_3$ , the films grown

on  $\text{SrTiO}_3$  are subject to tensile strain, resulting in a suppression of  $T_c$  compared to the bulk [15] and a magnetization vector  $M$  lying in the plane of the film [16]. We confirmed the in-plane orientation of  $M$  by measuring hysteresis loops at 300 K with the field  $H$  in the plane of the sample using a SQUID magnetometer (see the inset of Fig. 1).  $M$  as a function of  $T$  was measured for the film composition  $x = 0.3$  and its corresponding target material (Fig. 1).  $T_c$  for the film and the target material are 350 K and 373 K, respectively, with the target material displaying a  $T_c$  which is 23 K higher than that of the film.

We used MFM to image the magnetic domain patterns in our films. The microscope was operated in the tapping mode where the phase shift  $\phi$  of the oscillating cantilever was detected as the tip was scanned at a fixed height above the sample. The magnetic tips were magnetized along the long axis of the tips, which is perpendicular to the film plane. All the scans were done for zero external field. Since the films have an in-plane easy axis, the MFM will be sensitive to the regions where the magnetization vector is rotating, or - in other words - the magnetic domain walls (DW). Panel **B** of Fig. 2 shows a typical magnetic domain pattern for the  $\text{La}_{0.77}\text{Sr}_{0.23}\text{MnO}_3$  film around the artificial GB. Panel **A** is the corresponding atomic force microscope (AFM) image, which attests both to the sharpness of the DW as well as the smoothness ( $\lesssim 1$  nm root mean square (RMS) variation in thickness over a  $20 \mu\text{m} \times 20 \mu\text{m}$  area) of the film. We can clearly see a sharp magnetic DW that coincides with the artificial GB. In addition, there are magnetic DWs on opposite sides of the GB which are not nucleated along any feature visible in the AFM image. Although they meet at the artificial GB, they have different orientations on either side, which represent the crystal orientation of the underlying substrate and consequently that of the film itself. On the left side of the GB, the DWs are parallel or perpendicular to the GB. From the right side of the GB, a magnetic DW initially emanates at an angle of  $45^\circ$  rela-

tive to the GB. Because a  $45^\circ$  angle also characterizes the rotation of the crystal axes across the GB in the bicrystal substrate, this confirms that our  $\text{La}_{0.77}\text{Sr}_{0.23}\text{MnO}_3$  film is epitaxial and a bicrystal with an artificial GB coincident with that of the bicrystal substrate. The magnetization vectors of the magnetic domains in the film are coupled to the crystal axes of the substrate - as we cross the GB the magnetization vector has to rotate, and therefore it is natural to form a magnetic DW at the GB. Fig. 2 shows large magnetic domains at room temperature (RT). Their sidelengths are of order  $50 \mu\text{m}$ , much larger than the  $60 \text{ nm}$  film thickness.

We established the evolution of magnetic domains as a function of  $T$  for an  $x = 0.3$  bicrystal film by imaging the domains using the MFM with the sample mounted on a variable  $T$  sample stage [17]. As shown in the left column of Fig. 3, raising  $T$  towards  $T \simeq T_c$  (panel **B**) reduces the magnetic contrast which exists at RT (panel **A**). As we increase  $T$  further, above  $T_c$ , we notice a remarkable thing - the emergence of a new magnetic region (indicated by blue in panel **C**), very different from the domain pattern observed below  $T_c$ . Specifically, at  $355\text{K}$ , there is a distinct mesoscale region along the GB, with a half-width of approximately  $0.7 \mu\text{m}$ . At  $T = 360 \text{ K}$ , the mesoscale region shrinks to a half-width of  $0.5 \mu\text{m}$  and it disappears entirely at  $T = 370 \text{ K}$ . The effect is observed not only at the artificial GB (which was introduced intentionally) but also at other locations on the film (see right column of Fig. 3), where there are naturally occurring substrate defects. These defects can be clearly seen in the topography (AFM) channel. In such a location, we followed the evolution of the magnetic images in smaller  $T$  increments. The  $T$  dependence of the new magnetic region is the same as that around the artificial GB. It appears at  $T \gtrsim T_c$ , peaks at  $360 \text{ K}$ , and vanishes at  $370 \text{ K}$ .

To quantify the magnetic contrast, we calculated the RMS of  $\phi$  in the MFM image at each  $T$ , where  $\phi_{rms} = \sqrt{\langle (\phi(x, y) - \phi_{av})^2 \rangle}$ .  $\phi(x, y)$  represents the phase shift at each pixel and  $\phi_{av}$  is the average phase shift in the MFM image. The results are plotted in Fig. 4C. The magnetic contrast between the mesoscale region (indicated by blue in panels **C**, **D**, **G**, and **H**) and the rest of the sample (indicated by yellow and green in **C**, **D**, **G**, and **H**) arises because the mesoscale region is ferromagnetic (FM) and the rest is paramagnetic (PM) at  $T \gtrsim T_c$ . When both the mesoscopic region and the bulk part of the film are FM (when  $T < T_c$ , i.e. at  $300 \text{ K}$ ), the magnetization vector has a large magnitude, and therefore the interaction between the tip and the sample is strong, resulting in a large magnetic contrast in the MFM image at regions where the magnetization vector rotates (i.e., at the DWs). When the film becomes weakly FM (when  $T \sim T_c$ ), the interaction between the tip and the sample is weak all across the sample. Therefore, the variation of  $\phi$  across the scanned image is small resulting in a small

$\phi_{rms}$ . As the ferromagnetism of the bulk part diminishes, the difference in magnetic force between the mesoscopic region (FM) and the rest of the sample (PM) increases as shown in Fig. 4C. At  $T > T_c$ , the regions away from the GBs become PM, whereas the regions near the GBs stay FM. There is then a large difference in the magnetic force experienced by the tip in the two regions, which gives rise to a large variation of  $\phi$  across the image, resulting in a large  $\phi_{rms}$ . Eventually, the difference in magnetic force between the two regions decreases and vanishes as the ferromagnetism of the mesoscopic region vanishes and the whole film becomes PM.

It is notable that the new magnetic regions above  $T_c$  are magnetized in one direction when imaged with the MFM (as evidenced by the dominant blue color in the images) and the force between the tip and these FM regions is always attractive. We believe that the tip magnetizes these regions in a direction perpendicular to the film plane as it scans the sample. This is likely to happen given that these regions are soft magnets with a small coercive field ( $H_c \lesssim 8 \text{ G}$ ), as described below and shown in Fig. 4B. From the images,  $T_c$  can be mapped spatially by locating the FM-PM boundary as a function of  $T$  since at the boundary  $T = T_c$  (Fig. 4A). That the mesoscopic regions shrink as  $T$  is raised shows that  $T_c$  varies spatially, with the regions closer to the grain boundary having a higher  $T_c$ .

We have discovered that a thin manganite film has inhomogeneous magnetic properties due to both natural and artificial GBs. Because the GBs, especially when the micron scale healing length observed directly in the MFM images is taken into account, occupy an appreciable volume of the film, we expect to see evidence for ferromagnetism extending up to  $370 \text{ K}$  in very sensitive bulk magnetization measurements. Therefore, we have measured hysteresis loops using SQUID magnetometry. Indeed, we found that although the  $T$  dependence of the order parameter indicates a  $T_c = 350 \text{ K}$  for  $x = 0.3$  film composition, there is still a tiny hysteresis left at  $T \gtrsim T_c$  (see Fig. 4B). The tiny hysteresis loops close exactly at the same temperature ( $T = 370 \text{ K}$ ) at which the mesoscale regions disappear in the MFM image. The hysteresis loops at  $T \gtrsim T_c$  have the same shape whether the field is applied in the plane or perpendicular to the plane of the film. This indicates that the FM regions around the GBs are isotropic, in contrast to the rest of the film, which shows an in-plane easy axis throughout the whole  $T$  range including the vicinity of  $T_c$ .

We also measured magnetization loops in the bulk powder (ceramic) target  $\text{La}_{0.7}\text{Sr}_{0.3}\text{MnO}_3$  from which the film was grown. Hysteresis ceases at  $370 \text{ K}$ , which is also the Curie temperature deduced from  $M$  versus  $T$  data (see Fig. 1). Therefore, the FM regions that exist at the GBs at  $T > T_c$  in the film do not exist in the bulk ceramic sample. If we compare the magnetization per unit volume for the film to that of the bulk powder target for

temperatures above  $T_c$  of the film, we can estimate the volume fraction of the film which is FM at these temperatures. At  $T = 355, 360,$  and  $365$  K, which are intermediate between the nominal Curie temperatures of the film and the powder, the FM volume fractions are 0.03, 0.02, and 0.01, respectively. These values are consistent with an estimate ( $0.02 = 1 \mu\text{m}$  width/ $50 \mu\text{m}$  distance between GBs) of the volume fraction occupied by mesoscale FM regions in the film, and so indicate that the small “foot” in  $M(T)$  above  $T_c$  for the film (see Fig. 1) is actually due to GB magnetism. Almost needless to say, in the absence of our MFM data, the foot would have many possible interpretations.

We attribute the variation of local  $T_c$  to the local variation of strain in the film. The effect of strain on the  $T_c$  of CMR films has been reported by various groups [18–20] and is by now a well-accepted phenomenon. Depending on the lattice mismatch between the film and the substrate, the strain on the film can be modulated, which in turn modulates  $T_c$  substantially. This phenomenon has been attributed to the Jahn-Teller distortion arising from biaxial strain [18]. The coincidence of Curie temperatures and the magnetization per unit volume make it very likely that the mesoscale regions in our films are very similar to the bulk starting material. Therefore, near the GBs, the film is strain relieved leading to a  $T_c$  almost the same as that of the bulk. On the other hand, away from these crystal imperfections, the film is under tensile strain and its  $T_c$  is suppressed by 20 K. The width of the mesoscale region is an indication of the range over which strain propagates from the GB.

To summarize, we have discovered distinctive magnetic properties - most notably a higher Curie temperature - in mesoscale regions around GBs in manganites. The distinctive properties obtain whether the GBs occur naturally in unplanned fashion, or are introduced deliberately via a bicrystal substrate. They therefore need to be incorporated in descriptions of the electronic transport in all CMR films. Instead of sharp boundaries that divide crystal grains, one needs to consider separate regions around the GBs, which may have not only different magnetic properties, but also different electronic structures. A magnetically disordered region or mesoscale region around the GBs has been invoked [4,5,7] to explain magnetotransport results, which could not be explained by SPT at a sharp interface. Our results represent the first direct evidence that the interfaces have magnetic properties which are actually modulated over mesoscopic distances. Beyond its implications for a topic of great current interest, namely exploiting GBs for electronic devices, our experiment is significant because it is pioneering in the sense of imaging a spatially varying Curie temperature and using force microscopy as a quantitative tool in the study of a  $T$ -dependent magnetic phenomenon.

## ACKNOWLEDGMENTS

We are very grateful to Peter Littlewood for helpful discussions and the contacts which made this collaboration possible, as well as to Chang-Yong Kim for valuable X-ray analysis of our films.

- 
- [1] H. L. Ju *et al.*, Phys. Rev. B **51**, 6143 (1995).
  - [2] P. Schiffer *et al.*, Phys. Rev. Lett. **75**, 3336 (1995).
  - [3] H. Y. Hwang *et al.*, Phys. Rev. Lett. **77**, 2041 (1996).
  - [4] A. Gupta *et al.*, Phys. Rev. B **54**, R15629, (1996).
  - [5] J. E. Evetts *et al.*, Philos. Trans. R. Soc. London, Ser. A **356**, 1593 (1998).
  - [6] L. Balcells *et al.*, Phys. Rev. B **58**, R14697 (1998).
  - [7] J. Klein *et al.*, Europhys. Lett. **47**, 371 (1999).
  - [8] N. D. Mathur *et al.*, Nature (London) **387**, 266 (1997).
  - [9] K. Steenbeck *et al.*, Appl. Phys. Lett. **71**, 968 (1997).
  - [10] S. P. Isaac *et al.*, Appl. Phys. Lett. **72**, 2038 (1998).
  - [11] S. Jin *et al.*, Science **264**, 413 (1994).
  - [12] P. Lecoeur *et al.*, J. Appl. Phys. **82**, 3934 (1997).
  - [13] D. K. Petrov *et al.*, J. Appl. Phys. **83**, 7061 (1998).
  - [14] Z. W. Lin *et al.*, Appl. Phys. Lett. **74**, 3014 (1999).
  - [15] F. Tsui *et al.*, Appl. Phys. Lett. **76**, 2421 (2000).
  - [16] C. Kwon *et al.*, J. Magn. Magn. Mater. **172**, 229 (1997).
  - [17] Y. Soh and G. Aeppli, J. Appl. Phys. **85**, 4607 (1999).
  - [18] A. J. Millis, T. Darling, and A. Migliori, J. Appl. Phys. **83**, 1588 (1998).
  - [19] Q. Gan *et al.*, Appl. Phys. Lett. **72**, 978 (1998).
  - [20] R. A. Rao *et al.*, J. Appl. Phys. **85**, 4794 (1999).

FIG. 1.  $M$  versus  $T$  of  $\text{La}_{0.7}\text{Sr}_{0.3}\text{MnO}_3$  film and bulk powder sample. For the film,  $H$  was 20 G ( $>$  coercive field) and was applied in the plane of the sample and perpendicular to the grain boundary. For the bulk powder sample which had a needle shape,  $H$  was 500 G and was applied along the long axis of the sample. The  $T_c$  of the film is 350 K, which is 23 K lower than the  $T_c = 373$  of the powder target material. The inset shows the magnetic hysteresis loop of the film at 300 K, with the field applied in the plane of the film and perpendicular to the grain boundary.

FIG. 2. Room temperature AFM and MFM images of the region around the artificial grain boundary in the  $\text{La}_{0.77}\text{Sr}_{0.23}\text{MnO}_3$  film grown on a bicrystal  $\text{SrTiO}_3$  (001) substrate. The scan size is  $74 \mu\text{m}$  for both images. **A** The AFM image shows the topography of the film, which indicates the presence of an artificial grain boundary. The  $z$  scale is in units of nm. **B** The MFM image displays the magnetic domain walls in the system, one of which coincides with the artificial grain boundary. The  $z$  scale represents the phase shift of the oscillating cantilever in degree units.

FIG. 3. Evolution of magnetic pattern in the  $\text{La}_{0.7}\text{Sr}_{0.3}\text{MnO}_3$  film around the artificial grain boundary and around natural defects as a function of  $T$ . Images **A**, **B**, **C**, and **D** were taken around the artificial grain boundary at 300, 350, 355, and 365 K, respectively. The scan size for these images was  $5\ \mu\text{m}$  and a common  $z$  scale was used, which is displayed at the left of the images in degree units. Images **E**, **F**, **G**, and **H** display the magnetic pattern around natural defects at 300, 350, 355, and 365 K, respectively. The scan size for this region was  $14\ \mu\text{m}$ . The  $z$  scale for the scans is displayed at the right of the image in degree units. As  $T$  is raised from 300 K, the magnetic contrast diminishes. As  $T$  is raised above  $T_c$ , a new magnetic region emerges around the grain boundary. The width and strength of this new magnetic region evolves as a function of  $T$ . The region eventually vanishes at  $T = 370$  K.

FIG. 4. Comparison between magnetic information derived from MFM measurements and standard bulk magnetometry data. **A** Dependence of  $T_c$  on distance from artificial grain boundary, as established from the MFM images in Fig. 3. **B** Magnetic hysteresis loops of the  $\text{La}_{0.7}\text{Sr}_{0.3}\text{MnO}_3$  film for  $T > T_c$  were measured with the magnetic field applied in the plane of the film and perpendicular to the artificial grain boundary. The loops, which are open at  $T < 370$  K, close at 370 K. **C** Left axis shows the magnetic contrast of the MFM images in Fig. 3 represented by the RMS of  $\phi$  in the MFM signal as a function of  $T$ . This is compared against the quantity plotted on the right axis, which is the coercive field of the  $\text{La}_{0.7}\text{Sr}_{0.3}\text{MnO}_3$  film at  $T > T_c$  extracted from the magnetic hysteresis loops in panel **B**. The two quantities show a similar  $T$  dependence. The solid line is a smooth fit of the RMS of  $\phi$  and serves as a guide to the eye.

This figure "lsmofig1m.gif" is available in "gif" format from:

<http://arxiv.org/ps/cond-mat/0007169v1>

This figure "lsmofig2m.jpg" is available in "jpg" format from:

<http://arxiv.org/ps/cond-mat/0007169v1>

This figure "lsmofig3m.jpg" is available in "jpg" format from:

<http://arxiv.org/ps/cond-mat/0007169v1>

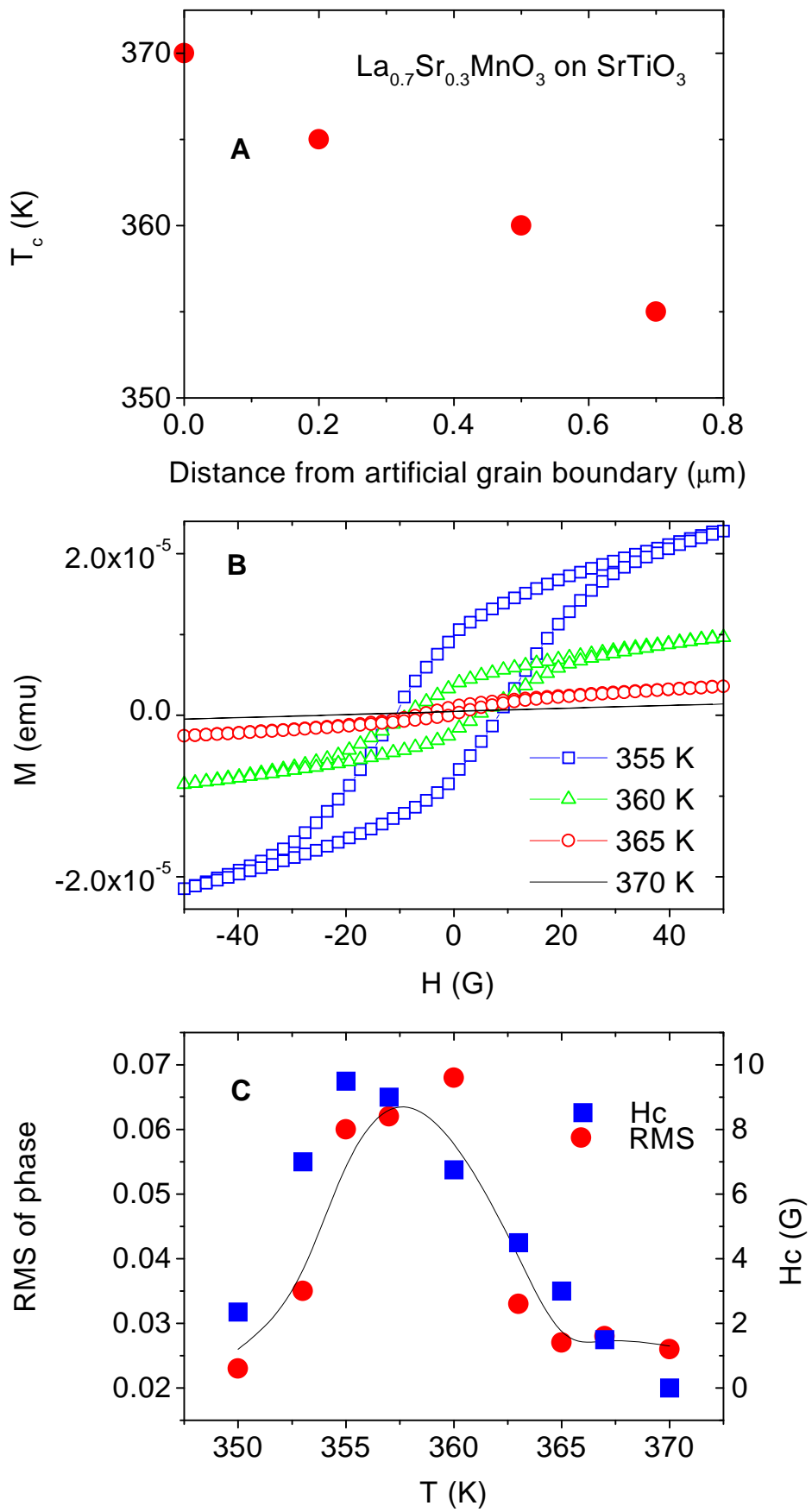


Fig.4 Soh *et al.*